A DFT-Based UTD Ray Analysis of Large Finite Phased Arrays on a Grounded Substrate

Panuwat Janpugdee, *Student Member, IEEE,* and Prabhakar H. Pathak, *Fellow, IEEE*

***Abstract*—A discrete Fourier transform (DFT)-based asymptotic high-frequency, uniform geometrical theory of diffraction (UTD) ray solution is developed to describe, in closed form, the collective field produced by large finite phased arrays of printed antenna elements on a grounded material substrate. Such a DFT-UTD ray analysis yields useful physical insights into the large array radiation and scattering mechanisms. This is in contrast to the conventional array element-by-element summation for the radiated field which lacks the above useful properties. In the present work, any realistic arbitrary array current distribution, i.e., in the presence of array mutual coupling, is represented by a DFT expansion so that each term in the expansion becomes a simple uniform array distribution with a linear phase, which then directly facilitates the development of the asymptotic UTD ray solution. Furthermore, another significant advantage of the DFT is that for most practical array excitations, only a relatively few DFT terms remain dominant in the expansion and are sufficient to provide reasonably accurate results. Some numerical examples are presented to illustrate the utility of this collective DFT-based asymptotic UTD ray solution for large array fields.**

***Index Terms*—Discrete Fourier transform (DFT), phased arrays, uniform geometrical theory of diffraction (UTD).**

I. Introduction

LARGE, periodic, finite phased printed antenna arrays are being increasingly utilized in electromagnetic sensor and communication systems. For example, such antenna arrays are attractive for aerospace, satellite, and shipboard applications, which require antennas with relatively high gain, low profile, and electronic beam steering capability. It is therefore of interest to develop an efficient as well as physically appealing analysis of such large finite periodic printed antenna arrays. With this view in mind, a uniform geometrical theory of diffraction (UTD) solution is developed for expressing the collective radiation from an entire large finite printed array at once in terms of a relatively few rays, as opposed to the far less efficient conventional array element-by-element field summation approach which also fails to provide a physical picture into the collective array radiation mechanisms.

The infinite periodic array solution, which allows the representation of the fields in terms of the Floquet modal expansion [1], provides a highly efficient computation of the array radiation far away from the array face due to the rapidly convergent property of the Floquet expansion. However, the infinite periodic array solution does not fully describe the behavior of finite arrays, even when they are large, since it omits the important effects resulting from finite array truncation, which can significantly modify the element input impedances, especially for elements near the edges of the finite array, and can also affect the radiation in all directions. In [2]–[4], some useful, initial approaches were developed for analyzing the collective fields associated with finite arrays; however, they all require a numerical treatment involving more complex series and integrals, in contrast to closed form ray solutions. Ray solutions have been developed previously for a two-dimensional (2-D) finite array [5], [6], a semi-infinite array [7], as well as a planar three-dimensional (3-D) finite array [8], [9], respectively, for free-standing arrays in air. Additional ray solutions have also been developed for 2-D finite array of filamentary line sources on a grounded material slab [10], and for a semi-infinite array of printed dipoles [11]. Since the work in [11] deals with a semi-infinite array configuration, only array edge effects are present in that case. In contrast, this paper deals with a fully finite 3-D array configuration which contains both finite array edges and corners, hence it also includes array corner effects which are not available in [11].

In all previous ray analyses, the assumption of a simple and smooth, as well as relatively slowly varying array current distribution is required. It is noted that the asymptotic ray analysis cannot directly deal with a realistic array current distribution which in general is nonsmooth, and typically has noticeable ripples that become even more pronounced near the array edges and corners. These ripples may be viewed as resulting from an interference between the waves generated by the array interior as if the array was infinite, and the diffracted waves generated by the finite array element truncation boundary. Hence, it becomes necessary to represent such realistic, complex array distributions by a sequence of simpler distributions which then become amenable to a collective array radiation analysis based on the UTD ray concept. In the present work, a relatively arbitrary, realistic array current distribution is represented in an exact fashion by a discrete Fourier transform (DFT) expansion. The realistic array current distribution is found, for a given array excitation, using an exact formulation that can be solved via numerical techniques such as the method of moments (MoM) or the more efficient accelerated DFT-MoM [12], [13]. The MoM solution contains mutual coupling effects between all array elements. Since each term of the finite DFT representation becomes a simple uniform distribution with a linear phase, it hence facilitates the asymptotic high frequency analysis that leads to a closed form ray solution for the collective array radiation which can be cast in the UTD form. The total field can then be computed by the superposition of asymptotic UTD ray fields due to

Manuscript received September 30, 2004; revised October 14, 2005. This work was supported in part by Temasek Laboratories, National University of Singapore.

The authors are with the ElectroScience Laboratory, the Department of Electrical and Computer Engineering, The Ohio State University, Columbus, OH 43212 USA (e-mail: janpugdee.1@osu.edu; pathak.2@osu.edu).

Digital Object Identifier 10.1109/TAP.2006.872595

all DFT terms. Although the number of terms in the DFT expansion of the array current distribution are exactly the same as the number of array elements, it can be shown indirectly from the ray solution that only a relatively few DFT terms remain significant for almost all practical array excitations. Thus, it is possible to truncate the complete DFT expansion and retain only the relatively few significant DFT terms to provide an efficient solution. For rectangular planar arrays, the dominant DFT spectrum components are located in the two narrow principle spectral bands. For other array shapes made up of piecewise linear boundaries, a few additional bands may be required. A typical example of the DFT spectrum of the array current distribution for a rectangular array boundary is shown in Fig. 10. Generally, the DFT expansion is truncated to approximately between 10% to 20% of the total number (which equals the total number of array elements) based on numerical experimentation with most practical array distributions. A sliding window (SLW) DFT approach which adds only a few additional spectra allows increased accuracy if so desired. In that case, a small window containing a few additional DFT terms is centered at a given aspect of observation, and it then slides or moves with the observer location.

In the present work, the 2-D analysis of [10] is extended to deal with the fully 3-D problem of a finite rectangular planar phased array of printed antenna elements on an infinite grounded material slab. The present UTD ray solution, which was summarized previously in a conference presentation by the authors [14], describes the surface and leaky waves (SW/LWs) excited by such fully 3-D finite arrays. The fully 3-D finite array geometry treated here introduces additional complexity over the 2-D finite array and 3-D semi-infinite array cases due to the interactions between several types of waves that are caused by the presence of corners. In particular, this work includes array corner effects, namely the corner-diffracted space wave and the corner-excited SW/LWs, which are not available in [11]. A uniform asymptotic ray solution for the edge-diffracted space wave and edge-excited SW/LWs presented in this paper is formally similar to that presented in [11]. The edge-diffracted space wave given in [11] contains the terms for the uniform compensation of the discontinuities in FWs and also SW/LWs; whereas the solution in this paper retains only the terms for the uniform compensation of FWs. For engineering purposes, the present solution provides a good approximation for the field at all observation points not very close to grazing aspects; while the omitted terms can always be added in a straightforward manner to yield a more rigorous asymptotic UTD solution if desired. In addition, the asymptotic UTD solution for the Floquet diffracted space wave contributions presented in this paper retains only the first order terms which vanish at the grazing aspect. For observation points at grazing, which are important when dealing with a hybrid UTD-MoM integral equation solution, the higher order terms of the asymptotic solution become significant and need to be included to obtain more accuracy [15]. However, the scope of this paper focuses on the collective radiation from the array for which the first order asymptotic solution is sufficiently accurate, and does not deal with a UTD solution useful in the approximate hybrid UTD-MoM solution for the array current distribution. Instead, the array current distribution is obtained in this paper via a rigorous and more accurate accelerated DFT-MoM formulation [12], [13], which is also efficient and has demonstrated that a rectangular patch antenna array with as many as a million elements can be solved in less than one hour on a desktop personal computer (Pentium IV 2.4 GHz, 512 MB).

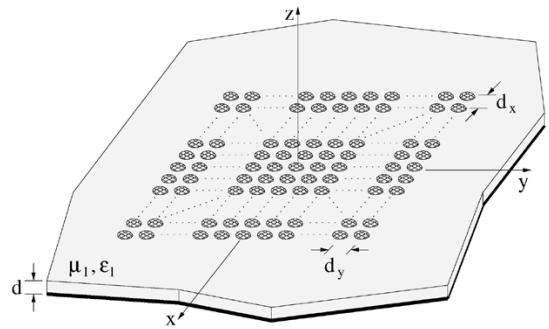

Fig. 1. Rectangular array of $(2N+1) \times (2M+1)$ printed antenna elements on an infinite grounded material slab.

The present method is directly applicable to any array of printed antenna elements and also to the scattering from such an array. The numerical example involving the radiation from a finite array of short and thin printed dipoles is presented in this paper just to simply illustrate the concepts of the DFT-UTD ray method. This DFT-UTD ray approach can also be extended to large nonrectangular array boundaries which can be represented by piecewise linear segments, as well as to quasiperiodic arrays and to finite planar arrays embedded in multi-layered media. These significant extensions mentioned above are beyond the scope of this paper, and as such, they will form the subject of a future paper, together with studies indicating that the DFT representation scales relatively well with increase in frequency (or array size). It may be remarked that a nonrectangular periodic array can also be treated as a sum of linear arrays; such a concept has been utilized recently in [16]. One notes that as an alternative to the DFT procedure described here, one can also form array element subgroups (or subarrays) for calculating the array fields more efficiently than the conventional brute force array element-by-element field summation. In the latter case, the size of the subarrays must be chosen so that the field point is in the far zone of the subarrays; however, such array element subgrouping does not scale with frequency (or array size).

This paper is organized as follows. In Section II, the DFT-based asymptotic UTD ray solution for the collective printed array radiation is developed. The closed form expressions for this asymptotic UTD solution are given in Section III, together with the physical picture that it provides for the whole array radiation in terms of just a few rays. In Section IV, numerical results of a finite phased array of short printed dipoles on a grounded dielectric substrate are illustrated for validating the accuracy and efficiency of the present DFT-UTD ray solution.

II. Formulation

Consider a large, finite rectangular array of $(2N+1)\times(2M+1)$ printed antenna elements on an infinite grounded material slab as shown in Fig. 1. The material slab has a thickness d, permeability $\mu_1 = \mu_r\mu_0$, and permittivity $\epsilon_1 = \epsilon_r\epsilon_0$, respectively, where (μ_0, ϵ_0) are the constitutive parameters of the free space.

The periodic interelement spacings in the $\hat{x}$ and $\hat{y}$ directions are d_x and d_y, respectively. The array is phased to radiate a main beam in the direction (θ_0, ϕ_0), where θ_0 and ϕ_0 are elevation and azimuth angles, respectively. It is noted that although the array of odd number of elements is considered here, the analysis for the case of even number of elements can be developed in a similar manner. An $e^{j\omega t}$ time convention for time-harmonic array sources and fields is assumed and suppressed throughout the development which follows.

The electric surface current distribution on the nmth printed antenna element is denoted by $\bar{J}_{nm}(\bar{r}')$, where $\bar{J}_{nm}(\bar{r}')$ can be represented in terms of a proper set of basis functions as

$$\bar{J}_{nm}(\bar{r}') \approx \left\{ \sum_{i=1}^{L} \bar{f}_i(\bar{r}') C_{nm,i} \right\} e^{-j(\beta_x n d_x + \beta_y m d_y)} \quad (1)$$

where $\bar{f}_i(\bar{r}')$ denotes the basis function and $C_{nm,i}$ is the corresponding unknown coefficient, which must be found via numerical methods such as the conventional MoM or the more efficient accelerated DFT-MoM [12], [13]. For the array of identical printed antenna elements, one can assume the same set of $\bar{f}_i(\bar{r}')$ for every antenna elements, which simplifies the analysis. In addition, $\beta_x = k_0 \sin\theta_0 \cos\phi_0$ and $\beta_y = k_0 \sin\theta_0 \sin\phi_0$ are the impressed scan phases of the array excitation in the $\hat{x}$ and $\hat{y}$ directions, respectively, which are factored out explicitly in the present analysis.

A. Spectral Representation of the Field

The electric field at an observation point $\bar{r}$ due to the nmth antenna element is given by the convolution integral of the dyadic Green's function $\bar{\bar{\Gamma}}(\bar{r}\,|\,\bar{r}')$ and the current distribution $\bar{J}_{nm}(\bar{r}')$ as

$$\bar{E}_{nm}(\bar{r}) = \int\int_{\Lambda_{nm}} \bar{\bar{\Gamma}}(\bar{r}\,|\,\bar{r}') \cdot \bar{J}_{nm}(\bar{r}')\, ds' \quad (2)$$

where Λ_{nm} denotes the domain of the current $\bar{J}_{nm}(\bar{r}')$ on the nmth antenna element.

The dyadic Green's function $\bar{\bar{\Gamma}}(\bar{r}\,|\,\bar{r}')$ for the electric field in the free space region (i.e., $z > 0$) is given in terms of a plane wave spectral representation by

$$\bar{\bar{\Gamma}}(\bar{r}\,|\,\bar{r}') = \frac{1}{4\pi^2} \int_{-\infty}^{\infty}\int_{-\infty}^{\infty} \bar{\bar{Q}}(k_x, k_y) e^{-j\bar{k}_0 \cdot (\bar{r} - \bar{r}')}\, dk_x\, dk_y \quad (3)$$

where

$$\bar{\bar{Q}}(k_x, k_y) = \left(\hat{k}_\rho - \hat{z}\frac{k_\rho}{\zeta_0} \right) \hat{k}_\rho Q_{\rm tm} + \hat{k}_t \hat{k}_t Q_{\rm te} \quad (4)$$

$$Q_{\rm tm} = \frac{\zeta_0 \zeta_1}{\omega \epsilon_0} \frac{\sin(\zeta_1 d)}{j\Delta_{\rm tm}}; \quad Q_{\rm te} = \omega \mu_1 \frac{\sin(\zeta_1 d)}{j\Delta_{\rm te}} \quad (5)$$

$$\Delta_{\rm tm} = \epsilon_r \zeta_0 \cos(\zeta_1 d) + j\zeta_1 \sin(\zeta_1 d) \quad (6)$$

$$\Delta_{\rm te} = \zeta_1 \cos(\zeta_1 d) + j\mu_r \zeta_0 \sin(\zeta_1 d) \quad (7)$$

The $\bar{k}_0 = \hat{x}k_x + \hat{y}k_y + \hat{z}\zeta_0$ and $\bar{k}_1 = \hat{x}k_x + \hat{y}k_y + \hat{z}\zeta_1$ are the vector wave numbers in the free space and material slab regions, respectively, where $|\bar{k}_0| = k_0 = \omega\sqrt{\mu_0 \epsilon_0}$ and $|\bar{k}_1| = k_1 = \omega\sqrt{\mu_1 \epsilon_1}$. The unit vectors $\hat{k}_\rho = \bar{k}_\rho / k_\rho$ and $\hat{k}_t = \hat{k}_\rho \times \hat{z}$, where $\bar{k}_\rho = \hat{x}k_x + \hat{y}k_y$.

The electric field radiated by the whole array is given initially via the array element-by-element field summation as

$$\bar{E} = \sum_{i=1}^{L} \left\{ \sum_{n=-N}^{N} \sum_{m=-M}^{M} \bar{E}_{nm,i} C_{nm,i} e^{-j(\beta_x n d_x + \beta_y m d_y)} \right\} \quad (8)$$

where

$$\bar{E}_{nm,i} = \frac{1}{4\pi^2} \int_{-\infty}^{\infty}\int_{-\infty}^{\infty} \bar{\bar{Q}}(k_x, k_y) \cdot \bar{F}_i(k_x, k_y) \cdot e^{-j\bar{k}_0 \cdot (\bar{r} - \bar{r}'_{nm})}\, dk_x\, dk_y \quad (9)$$

$$\bar{F}_i(k_x, k_y) = \int\int_{\Lambda_i} \bar{f}_i(\bar{r}'') e^{j\bar{k}_0 \cdot \bar{r}''}\, ds''. \quad (10)$$

The superscript $''$ denotes the local coordinate system centered at $\bar{r}'_{nm} = \hat{x}nd_x + \hat{y}md_y$, where $\bar{r}'_{nm}$ defines the reference point of the nmth antenna element. The Λ_i denotes the domain of $\bar{f}_i(\bar{r}'')$ in that local coordinate system.

The current basis functions $\bar{f}_i(\bar{r}')$ on every antenna elements form an individual mathematical periodic array. The total field radiated by the entire actual array can be obtained from a superposition of the fields produced by each of mathematical arrays formed by $\bar{f}_i(\bar{r}')$, for $i = 1, \ldots, L$. Hence, the present method is readily applicable to treat a finite array of arbitrary-shaped printed antenna elements as discussed above. However, for simplicity of the illustration of the concepts and formulation, the development to follow will assume, without loss of generality, a finite array of very tiny printed antenna elements such that the current distribution on each antenna element can be represented by a single basis function $\bar{f}(\bar{r}')$, i.e.

$$\bar{J}_{nm}(\bar{r}') \approx \bar{f}(\bar{r}') C_{nm} e^{-j(\beta_x n d_x + \beta_y m d_y)}. \quad (11)$$

It follows that the expression for the electric field in (8) reduces to:

$$\bar{E} = \sum_{n=-N}^{N} \sum_{m=-M}^{M} \bar{E}_{nm} C_{nm} e^{-j(\beta_x n d_x + \beta_y m d_y)} \quad (12)$$

where

$$\bar{E}_{nm} = \frac{1}{4\pi^2} \int_{-\infty}^{\infty}\int_{-\infty}^{\infty} \bar{\bar{Q}}(k_x, k_y) \cdot \bar{F}(k_x, k_y) \cdot e^{-j\bar{k}_0 \cdot (\bar{r} - \bar{r}'_{nm})}\, dk_x\, dk_y \quad (13)$$

$$\bar{F}(k_x, k_y) = \int\int_{\Lambda} \bar{f}(\bar{r}'') e^{j\bar{k}_0 \cdot \bar{r}''}\, ds''. \quad (14)$$

The $\bar{F}$ in (14) can be seen to be the Fourier transform of the current $\bar{f}$, and hence it is proportional to the element pattern.

The array distribution of the coefficients C_{nm} in (11) can be represented by a DFT expansion as

$$C_{nm} = \sum_{k=0}^{2N} \sum_{l=0}^{2M} \tilde{C}_{kl} e^{-j2\pi nk/(2N+1)} e^{-j2\pi ml/(2M+1)} \quad (15)$$

where $\tilde{C}_{kl}$ are the DFT coefficients given by

$$\tilde{C}_{kl} = \sum_{n=-N}^{N} \sum_{m=-M}^{M} C_{nm} e^{j2\pi nk/(2N+1)} e^{j2\pi ml/(2M+1)} \quad (16)$$

which can be found efficiently via the fast Fourier transform (FFT) [17].

By using the DFT expansion of (15) in (12), one obtains

$$\bar{E} = \sum_{k=0}^{2N}\sum_{l=0}^{2M} \tilde{C}_{kl}\bar{E}_{kl} \tag{17}$$

where $\bar{E}_{kl}$ is the electric field produced by the (k,l)th DFT component, which is given by

$$\bar{E}_{kl} = \frac{1}{4\pi^2}\int_{-\infty}^{\infty}\int_{-\infty}^{\infty} \bar{G}(k_x,k_y)e^{-j\bar{k}_0\cdot\bar{r}}S_x(k_x)S_y(k_y)\,dk_x\,dk_y \tag{18}$$

where

$$\bar{G}(k_x,k_y) = \bar{\bar{Q}}(k_x,k_y)\cdot\bar{F}(k_x,k_y) \tag{19}$$

$$S_x(k_x) = \sum_{n=-N}^{N} e^{j(k_x-\beta_x^k)nd_x} \tag{20}$$

$$S_y(k_y) = \sum_{m=-M}^{M} e^{j(k_y-\beta_y^l)md_y}. \tag{21}$$

The β_x^k and β_y^l are the DFT-modulated impressed phases in the $\hat{x}$ and $\hat{y}$ directions, respectively, which are given by

$$\beta_x^k = \beta_x + \frac{2\pi k}{(2N+1)d_x};\quad \beta_y^l = \beta_y + \frac{2\pi l}{(2M+1)d_y}. \tag{22}$$

As mentioned earlier, for most practical array distributions, only a relatively few DFT terms of the expansion in (15) are significant. Hence, the summation in (17) can be approximated by the truncated sum as

$$\bar{E} \approx \sum_{(k,l)\in D} \tilde{C}_{kl}\bar{E}_{kl} \tag{23}$$

where the $(k,l)\in D$ denote only the dominant DFT terms.

By utilizing the partial Poisson sum formula [5], [18], the finite element-by-element summations in (20) and (21) are converted into the infinite Floquet-type modal sums of finite Poisson spatial integrals plus the end point corrections. After evaluating the spatial integrals in closed form, one obtains

$$S_x = B_x^+(k_x)e^{j(k_x-\beta_x^k)Nd_x} + B_x^-(k_x)e^{-j(k_x-\beta_x^k)Nd_x} \tag{24}$$

$$S_y = B_y^+(k_y)e^{j(k_y-\beta_y^l)Md_y} + B_y^-(k_y)e^{-j(k_y-\beta_y^l)Md_y} \tag{25}$$

where

$$B_x^{\pm}(k_x) = \left\{\frac{1}{2} \pm \frac{1}{jd_x}\sum_{p=-\infty}^{\infty}\frac{1}{(k_x-k_x^p)}\right\} \tag{26}$$

$$B_y^{\pm}(k_y) = \left\{\frac{1}{2} \pm \frac{1}{jd_y}\sum_{q=-\infty}^{\infty}\frac{1}{(k_y-k_y^q)}\right\}. \tag{27}$$

The k_x^p and k_y^q are referred to as the Floquet wave numbers in the $\hat{x}$ and $\hat{y}$ directions, respectively, and are given by

$$k_x^p = \beta_x^k + \frac{2\pi p}{d_x};\qquad k_y^q = \beta_y^l + \frac{2\pi q}{d_y}. \tag{28}$$

The representations of $B_x^{\pm}(k_x)$ and $B_y^{\pm}(k_y)$ can be expressed in closed form as [5]

$$\begin{aligned} B_x^{\pm}(k_x) &= \frac{1}{2} \mp \frac{j}{2}\cot\left\{\frac{1}{2}(k_x-\beta_x^k)d_x\right\} \\ &= \mp\frac{je^{\pm\frac{j}{2}(k_x-\beta_x^k)d_x}}{2\sin\left[\frac{1}{2}(k_x-\beta_x^k)d_x\right]} \end{aligned} \tag{29}$$

$$\begin{aligned} B_y^{\pm}(k_y) &= \frac{1}{2} \mp \frac{j}{2}\cot\left\{\frac{1}{2}(k_y-\beta_y^l)d_y\right\} \\ &= \mp\frac{je^{\pm\frac{j}{2}(k_y-\beta_y^l)d_y}}{2\sin[\frac{1}{2}(k_y-\beta_y^l)d_y]}. \end{aligned} \tag{30}$$

Employing (24) and (25) in (18) yields

$$\bar{E}_{kl} = \sum_{i=1}^{4}\left\{\frac{e^{-j\psi_{c_i}}}{4\pi^2}\int_{-\infty}^{\infty}\int_{-\infty}^{\infty}\bar{G}(k_x,k_y)e^{-j\bar{k}_0\cdot\bar{r}_i} \cdot B_x^i(k_x)B_y^i(k_y)dk_xdk_y\right\} \tag{31}$$

where $B_x^i(k_x) = B_x^{\pm}(k_x), B_y^i(k_y) = B_y^{\pm}(k_y), \bar{r}_i = \bar{r} - \bar{r}'_{c_i}, \psi_{c_i} = \bar{\beta}_{kl}\cdot\bar{r}'_{c_i}, \bar{r}'_{c_i} = \pm\hat{x}Nd_x \pm \hat{y}Md_y$, and $\bar{\beta}_{kl} = \hat{x}\beta_x^k + \hat{y}\beta_y^l$, respectively. The $(+)$ or $(-)$ signs in the above parameters depend on the corresponding index, $i = 1,\ldots,4$.

B. Spectral Integral Evaluation

The integrand of the spectral integral in (31) has the following properties. The function $\bar{G}(k_x,k_y)$ has pole singularities due to the zeros of Δ_{tm} and Δ_{te} defined in (6) and (7), respectively. The poles which are located on (in the lossless case), or slightly off (in the lossy case), the real axis of the complex k_ρ plane on the proper Riemann sheet are referred to as the surface wave (SW) poles, since their residue contributions give rise to the proper SW contributions to the array fields. The poles which are located in the 2nd and 4th quadrants of the complex k_ρ plane, on the improper Riemann sheet, are referred to as the leaky wave (LW) poles since their residues yield array field contributions of the LW type. Furthermore, the functions $B_x^i(k_x)$ and $B_y^i(k_y)$ also contain pole singularities at $k_x = k_x^p$ and $k_y = k_y^q$, respectively. Those poles occur periodically in the complex k_x and k_y planes, respectively, and are referred to as the Floquet poles since their residue contributions give rise to the Floquet wave (FW) modes as in the infinite array case. Finally, the exponential function in (31) contains a first-order saddle point. The saddle point can contribute in conjunction with the Floquet poles or without. The Floquet poles and the saddle point contribute to the waves discussed in Sections III-A through III-C. Also, the waves arising from a coupling of Floquet and SW/LW poles are discussed in Section III-D, and the waves contributed from the SW/LW poles and the saddle point are discussed in Section III-E.

The spectral integral in (31) is evaluated by deforming the integration path into the steepest descent path (SDP), which is

evaluated asymptotically in closed form by using the steepest descent method [19] yielding the saddle point contribution; plus the contribution from the residues of all the poles which are enclosed by the contour deformation. The details of the asymptotic procedure, as well as the pole locations and the SDP in the complex planes, can be found in [20]. It is noted that a uniform asymptotic solution presented in this paper assumes that the FW poles do not interact with the SW/LW poles. This assumption is practical for most cases. However, in general, the SW/LW pole can possibly lie close to the FW pole so that their interactions need to be considered as discussed in more detail in [21], [22], only for the case of a semi-infinite array of printed dipoles. For a fully finite array of printed elements as encountered in this work, a more sophisticated uniform asymptotic procedure is required for developing a new corner transition function to deal with this rather special case; its development is beyond the scope of this paper. Alternatively, it may be possible to simply evaluate the generic integral numerically for this special case rather than in closed form via asymptotic approximations. These special cases will be investigated in the future.

III. Asymptotic Ray Fields

The asymptotic evaluation of the spectral integral in (31) yields the contributions to the total electric field, which arise from various critical points of the integrand, as follows [20]:

$$\bar{E} \approx \sum_{(k,l)\in D} \tilde{C}_{kl}\left[\bar{E}^{fw}_{kl} + \bar{E}^{d,e}_{kl} + \bar{E}^{d,c}_{kl} + \bar{E}^{slw,e}_{kl} + \bar{E}^{slw,c}_{kl}\right]. \tag{32}$$

Each term in (32) represents a collective UTD type ray field whose field expressions and physical interpretations are presented below.

A. Floquet Wave Modal Contributions

The contribution from the residues of the poles of $B^i_x(k_x)$ and $B^i_y(k_y)$ gives rise to the FWs

$$\bar{E}^{fw}_{kl} = \frac{1}{d_x d_y}\sum_{p=-\infty}^{\infty}\sum_{q=-\infty}^{\infty} \bar{G}\left(k^p_x, k^q_y\right) e^{-j\bar{k}^{pq}_0\cdot\bar{r}} U^{pq}_{fw}. \tag{33}$$

The FWs are in the form of a modal summation of plane waves with the wave number $\bar{k}^{pq}_0 = \hat{x}k^p_x + \hat{y}k^q_y + \hat{z}\zeta^{pq}_0$, where k^p_x and k^q_y are given by (28), and $\zeta^{pq}_0 = [k_0^2 - (k^p_x)^2 - (k^q_y)^2]^{1/2}$. The FWs represent the field produced by infinite periodic arrays. In finite arrays, each FW exists only within a confined region of space due to the array boundary truncation, and it therefore vanishes at the shadow boundary planes defined by the unit step function U^{pq}_{fw} which depends on the FW modal index (p, q). For a given frequency, generally only one or at most just a few lower order modes, which satisfy $(k^p_x)^2 + (k^q_y)^2 < k_0^2$, constitute modes that propagate away from the array face as shown in Fig. 2(a); whereas the remaining infinite number of modes, for which $(k^p_x)^2 + (k^q_y)^2 > k_0^2$, become evanescent above the array as shown in Fig. 2(b).

B. Floquet Edge-Diffracted Fields

The contribution from the residue of a Floquet pole of $B^i_x(k_x)$ (or $B^i_y(k_y)$) and the saddle point of the exponential term gives rise to the Floquet edge-diffracted fields from the $\hat{x}$-directed (or $\hat{y}$-directed) edge. The Floquet edge-diffracted field from the $\hat{x}$-directed edge e_i is given by

$$\bar{E}^{d,e_i}_{kl} = e^{-j\psi_{e_i}}\sum_p \bar{G}\left(k^p_x, k^p_{y,e_i}\right)\cdot\bar{\bar{D}}^p_{e_i}\frac{e^{-jk^p_{yz}\rho^{e_i}_{yz}}}{\sqrt{\rho^{e_i}_{yz}}} e^{-jk^p_x x} U^p_{d,e_i} \tag{34}$$

where

$$\bar{\bar{D}}^p_{e_i} = \frac{e^{j\pi/4}}{d_x\sqrt{2\pi k^p_{yz}}}\left\{\bar{\bar{D}}^{p,1}_{e_i} + \bar{\bar{D}}^{p,2}_{e_i}\right\} \tag{35}$$

$$\bar{\bar{D}}^{p,1}_{e_i} = \bar{\bar{I}}B^i_y\left(k^p_{y,e_i}\right)\zeta^p_{0,e_i} \tag{36}$$

$$\bar{\bar{D}}^{p,2}_{e_i} = -\frac{\varepsilon_{e_i}}{jd_y}\sum_q \bar{\bar{C}}^{pq}_{e_i}\frac{\left[1 - F\left(k^p_{yz}\rho^{e_i}_{yz}\left(\delta^{pq}_{yz,e_i}\right)^2\right)\right]}{\sqrt{2}\delta^{pq}_{yz,e_i}} \tag{37}$$

and

$$\bar{\bar{C}}^{pq}_{e_i} = \frac{\bar{G}\left(k^p_x, k^p_{y,e_i}\right)\bar{G}\left(k^p_x, k^q_y\right)}{\left|\bar{G}\left(k^p_x, k^p_{y,e_i}\right)\right|^2}. \tag{38}$$

The function $F(\cdot)$ in (37) is the UTD Fresnel type transition function [23] and its argument is given by

$$\delta^{pq}_{yz,e_i} = \sqrt{2}\sin\left(\frac{\xi^{pq}_{yz} - \phi^{e_i}_{yz}}{2}\right). \tag{39}$$

The U^p_{d,e_i} in (34) denotes the unit step function defining the shadow boundary of the Floquet edge-diffracted field. The $\bar{\bar{I}}$ in (36) denotes the identity dyadic. The corresponding wave numbers are defined as $k^p_{yz} = [k_0^2 - (k^p_x)^2]^{1/2}, k^p_{y,e_i} = k^p_{yz}\cos\phi^{e_i}_{yz}$, and $\zeta^p_{0,e_i} = k^p_{yz}\sin\phi^{e_i}_{yz}$. The other parameters are defined as $\xi^{pq}_{yz} = \cos^{-1}(k^q_y/k^p_{yz}), \phi^{e_i}_{yz} = \cos^{-1}((y - y'_{e_i})/\rho^{e_i}_{yz}), \rho^{e_i}_{yz} = [(y - y'_{e_i})^2 + z^2]^{1/2}, y'_{e_i} = \pm Md_y, \varepsilon_{e_i} = \mathrm{sgn}(y'_{e_i})$, and $\psi_{e_i} = \bar{\beta}_{kl}\cdot\hat{y}y'_{e_i}$. The Floquet edge-diffracted field from the $\hat{y}$-directed edge is in the form identical to the above expression but with the appropriate interchange of the x and y dependent variables.

In most cases, the SW/LW poles may not be sufficiently close to the saddle point. Hence, additional transition functions describing the behavior across the shadow boundaries of the corresponding edge-excited SW/LW, which are described in Section III-D, have been ignored here; however, they can be included as additional Fresnel type functions similar to that in (37) with an appropriate argument as in (39) except that the angles ξ and ϕ are now different, and ξ is complex for the SW/LW cases.

The Floquet edge-diffracted field arises from the diffraction of the FWs at the array edge caused by the abrupt array element truncation. The Floquet edge-diffracted field is in the form of modal conical waves emanating from the array edges. Each pth index of the Floquet edge-diffracted fields has a projected propagation constant along the edge which is matched to that of the FW undergoing the edge diffraction. Thus, the Floquet edge-diffracted field lies on a Keller cone of diffraction [24], whose half cone angle is defined by the phase matching condition $k\hat{s}_e\cdot\hat{x} = k^p_x$ (or $k\hat{s}_e\cdot\hat{y} = k^q_y$) for the $\hat{x}$-directed (or $\hat{y}$-directed) edge, where $\hat{s}_e$ is the direction from the edge diffraction point to the observer. The Floquet edge-diffracted field smoothly compensates the discontinuity of the associated Floquet mode which suddenly vanishes at the shadow boundary plane arising from that edge. The Floquet edge-diffracted field is composed of propagating modes $((k^p_x)^2 \text{or} (k^q_y)^2 < k_0^2)$ which

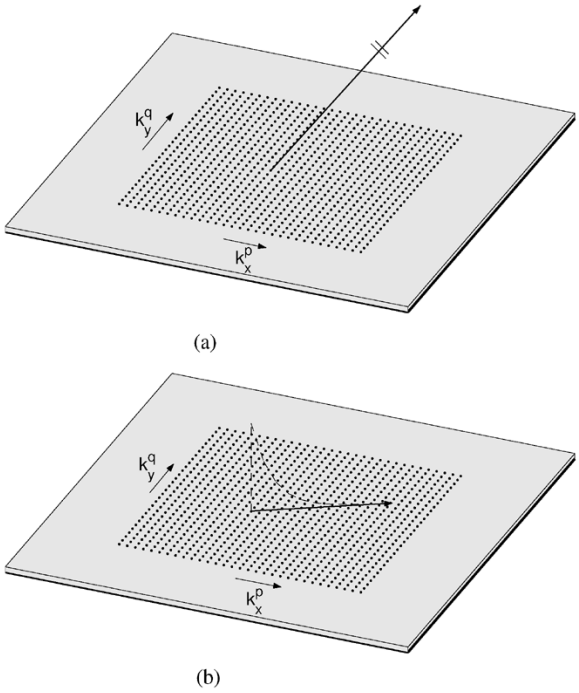

Fig. 2. Ray picture illustrating the Floquet wave. (a) Propagating mode and (b) evanescent mode.

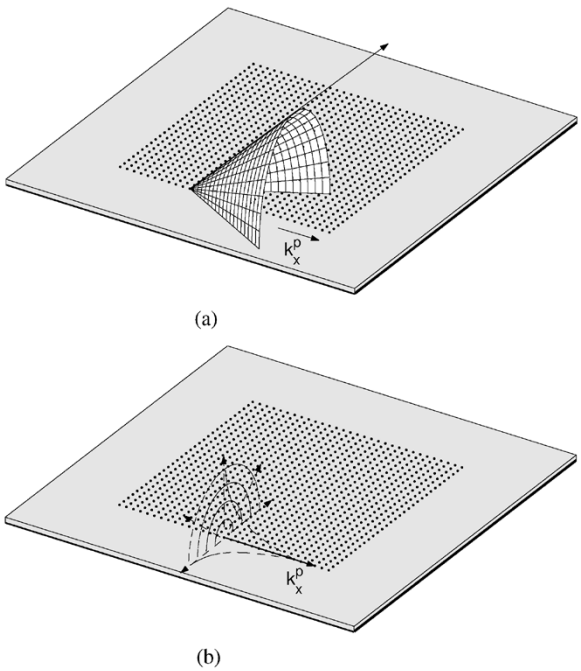

Fig. 3. Ray picture illustrating the Floquet edge-diffracted field. (a) Propagating mode and (b) evanescent mode.

diffract from the edge in the corresponding diffraction cones as in Fig. 3(a), and evanescent modes $((k_x^p)^2 \text{or} (k_y^q)^2 > k_0^2)$ which are guided along the edge while attenuating away from the edge as in Fig. 3(b). The Floquet edge-diffracted fields also exist within a confined region of space due to the truncation of the edge at the corner, while they vanish at the shadow boundary cones defined by the unit step function U^p_{d,e_i}.

C. Floquet Corner-Diffracted Fields

The contribution from the double saddle points of the exponential term yields the Floquet corner-diffracted fields. The Floquet corner-diffracted field from the corner c_i, formed by the junction of the $\hat{x}$-directed edge e_j and the $\hat{y}$-directed edge $e_{j'}$, respectively, is given by

$$\bar{E}^{d,c_i}_{kl} = e^{-j\psi_{c_i}} \bar{G}\left(k_x^{c_i}, k_y^{c_i}\right) \cdot \bar{\bar{D}}_{c_i} \frac{e^{-jk_0 r_i}}{r_i} \tag{40}$$

where

$$\bar{\bar{D}}_{c_i} = \frac{j}{2\pi}\left\{\bar{\bar{D}}^{(1)}_{c_i} + \bar{\bar{D}}^{(2)}_{c_i}\right\} \tag{41}$$

$$\bar{\bar{D}}^{(1)}_{c_i} = \bar{\bar{I}} B^i_x\left(k_x^{c_i}\right) B^i_y\left(k_y^{c_i}\right) \zeta_0^{c_i} \tag{42}$$

$$\begin{aligned}\bar{\bar{D}}^{(2)}_{c_i} = {} & \bar{\bar{I}} \frac{\varepsilon_{e_j}\varepsilon_{e_{j'}}}{d_x d_y} \zeta_0^{c_i} \sum_p \sum_q \frac{\left[1 - T\left(k_x^{c_i}, k_y^{c_i}; k_x^p, k_y^q\right)\right]}{\left(k_x^{c_i} - k_x^p\right)\left(k_y^{c_i} - k_y^q\right)} \\ & + \frac{\varepsilon_{e_{j'}}}{jd_x} \sum_p \bar{C}^p_{c_i,e_j} \frac{\zeta^p_{0,e_j}}{\sqrt{k^p_{yz} k^{c_i}_{yz}}} \frac{\left[1 - F\left(k_0 r_i \left(\Omega^p_{e_j}\right)^2\right)\right]}{2\Omega^p_{e_j}} \\ & + \frac{\varepsilon_{e_j}}{jd_y} \sum_q \bar{C}^q_{c_i,e_{j'}} \frac{\zeta^q_{0,e_{j'}}}{\sqrt{k^q_{xz} k^{c_i}_{xz}}} \frac{\left[1 - F\left(k_0 r_i \left(\Omega^q_{e_{j'}}\right)^2\right)\right]}{2\Omega^q_{e_{j'}}}\end{aligned} \tag{43}$$

and

$$\bar{\bar{C}}^p_{c_i,e_j} = \frac{\bar{G}\left(k_x^{c_i}, k_y^{c_i}\right) \bar{G}\left(k_x^p, k^p_{y,e_j}\right)}{\left|\bar{G}\left(k_x^{c_i}, k_y^{c_i}\right)\right|^2} \tag{44}$$

$$\bar{\bar{C}}^q_{c_i,e_{j'}} = \frac{\bar{G}\left(k_x^{c_i}, k_y^{c_i}\right) \bar{G}\left(k^q_{x,e_{j'}}, k_y^q\right)}{\left|\bar{G}\left(k_x^{c_i}, k_y^{c_i}\right)\right|^2}. \tag{45}$$

The function $T(\cdot)$ in (43) denotes the corner transition function [25]. The arguments of the $F(\cdot)$ function in (43) are given by

$$\Omega^p_{e_j} = \sqrt{2}\sin\left(\frac{\gamma_x^p - \theta_x^{c_i}}{2}\right); \quad \Omega^q_{e_{j'}} = \sqrt{2}\sin\left(\frac{\gamma_y^q - \theta_y^{c_i}}{2}\right) \tag{46}$$

where $\gamma_x^p = \cos^{-1}(k_x^p/k_0)$ and $\gamma_y^q = \cos^{-1}(k_y^q/k_0)$.

The corresponding wave numbers are defined as

$$k_x^{c_i} = k_0 \cos\theta_x^{c_i}; \quad k_{yz}^{c_i} = k_0 \sin\theta_x^{c_i} \tag{47}$$

$$k_y^{c_i} = k_0 \cos\theta_y^{c_i}; \quad k_{xz}^{c_i} = k_0 \sin\theta_y^{c_i} \tag{48}$$

$$\zeta_0^{c_i} = k_0 \cos\theta_z^{c_i}. \tag{49}$$

The other parameters are defined as $\theta_x^{c_i} = \cos^{-1}((x - x'_{c_i})/r_i), \theta_y^{c_i} = \cos^{-1}((y - y'_{c_i})/r_i), \theta_z^{c_i} = \cos^{-1}(z/r_i), x'_{c_i} = \pm N d_x, y'_{c_i} = \pm M d_y, r_i = [(x - x'_{c_i})^2 + (y - y'_{c_i})^2 + z^2]^{1/2}, \varepsilon_{e_j} = \text{sgn}(y'_{c_i})$, and $\varepsilon_{e_{j'}} = \text{sgn}(x'_{c_i})$, respectively. Also, $\{k^p_{yz}, k^p_{y,e_j}, \zeta^p_{0,e_j}\}$ and $\{k^q_{xz}, k^q_{x,e_{j'}}, \zeta^q_{0,e_{j'}}\}$ are defined as in Section III-B.

Again, the transition functions for the corresponding corner-excited SW/LW, which are described in Section III-E, are ignored for the same reasons as discussed in Section III-B for the edge-excited SW/LW contributions; however, they can be included by adding terms similar to those in (43).

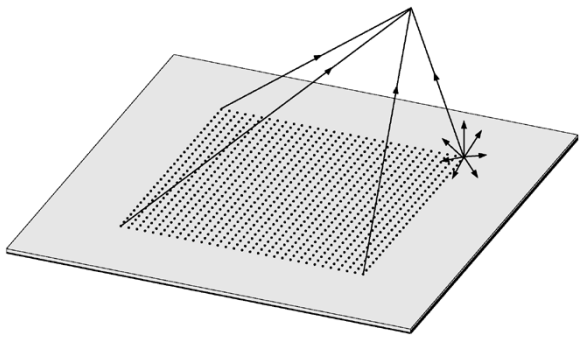

Fig. 4. Ray picture illustrating the Floquet corner-diffracted field.

The Floquet corner-diffracted fields arise from the diffraction of the FW due to the array boundary truncation at the corners. It is in the form of a spherical wave emanating from the corners of the array as shown in Fig. 4. The Floquet corner-diffracted fields smoothly compensate the discontinuity of the Floquet edge-diffracted fields at the corresponding shadow boundary cones arising at the corner, and also simultaneously compensate the discontinuity of the FWs at the overlap of shadow boundaries, which occurs when the two shadow boundary planes of the FWs coincide with the two shadow boundary cones of the Floquet edge-diffracted fields.

D. Floquet Edge-Excited Surface and Leaky Waves

The contribution from the residues of the SW/LW pole of $\bar{G}(k_x, k_y)$ and of the Floquet pole of $B_x^i(k_x)$ (or $B_y^i(k_y)$) gives rise to the Floquet edge-excited SW/LW. The SW/LW excited from the $\hat{x}$-directed edge e_i via Floquet edge diffraction is given by

$$\bar{E}_{kl}^{slw,e_i} = e^{-j\psi_{e_i}} \sum_m \sum_p \bar{R}_{e_i}^{mp} \cdot \bar{\bar{L}}_{e_i}^{mp} e^{-j\bar{k}_0^{mp}\cdot\bar{r}_{e_i}} U_{e_i}^{mp} \quad (50)$$

where

$$\bar{R}_{e_i}^{mp} = \mathrm{Res}\{\bar{G}\}\big|_{(k_\rho = k_\rho^m, k_x = k_x^p)} \quad (51)$$

$$\bar{\bar{L}}_{e_i}^{mp} = \bar{\bar{I}} \frac{k_\rho^m \zeta_0^m}{j d_x k_y^{mp}} B_y^i\left(k_y^{mp}\right) \quad (52)$$

$$\bar{k}_0^{mp} = \hat{x} k_x^p + \hat{y} k_y^{mp} + \hat{z}\zeta_0^m \quad (53)$$

$$k_y^{mp} = [(k_\rho^m)^2 - (k_x^p)^2]^{1/2}. \quad (54)$$

Also, $\bar{r}_{e_i} = \hat{x}x + \hat{y}|y - y'_{e_i}| + \hat{z}z$, where y'_{e_i} is defined as in Section III-B.

In the above expressions, m is the modal index of the SW/LWs. The $U_{e_i}^{mp}$ in (50) denotes the unit step function defining the shadow boundary of the edge-excited SW/LW modes. The $\mathrm{Res}\{\cdot\}$ in (51) denotes the residue of the function in the bracket. The k_ρ^m and ζ_0^m are the propagation constants of the SW/LWs in the directions along and normal to the surface, respectively. For the SW modes, k_ρ^m is real and greater than k_0 whereas ζ_0^m is purely imaginary; while for the LW modes, k_ρ^m and ζ_0^m are both complex. The expressions of the edge-excited SW/LWs from the $\hat{y}$-directed edge are identical to the above expressions but with the proper interchange of the x and y dependent variables.

The SW/LWs are excited from the array edges by Floquet edge diffraction. These SW/LW modes are similar to those that can exist in the grounded substrate in the absence of the array [26]. Fig. 5 shows the edge-excited SW/LW contribution for a given (m, p). Fig. 6(a) and (b) show the propagation and attenuation directions of the SW and LW above the grounded substrate, respectively. In Fig. 6(a), $\beta = k_\rho^m$ and $-j\alpha = \zeta_0^m$, respectively; whereas in Fig. 6(b), $\beta = \sqrt{(\mathrm{Re}[k_\rho^m])^2 + (\mathrm{Re}[\zeta_0^m])^2}$ and $\alpha = \sqrt{(\mathrm{Im}[k_\rho^m])^2 + (\mathrm{Im}[\zeta_0^m])^2}$. In general, more than one SW modes can be excited depending on the relative dielectric constant ϵ_r and the thickness d of the grounded slab for a given frequency range; while in some configurations, the LW can also be excited in addition to the SW. The edge-excited SW/LWs exist in a certain region as do the edge-diffracted Floquet waves and suddenly disappear at the shadow boundary due to the truncation of the edge, which is defined by the unit step function $U_{e_i}^{mp}$ in (50). There is no spreading of the edge-excited SW/LWs and their propagation constant is matched to the Floquet modal wave number in the direction along the edge. The traveling SW modes, of which $(k_\rho^m)^2 > (k_x^p)^2 \mathrm{or} (k_y^q)^2$, are launched and spread away from the array edge; while the edge-guided SW modes, of which $(k_\rho^m)^2 < (k_x^p)^2$ or $(k_y^q)^2$, are excited and guided along the array edge, and attenuate away from the edge.

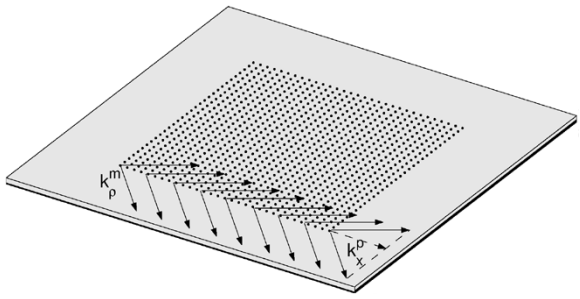

Fig. 5. Ray picture illustrating the edge-excited surface/leaky wave.

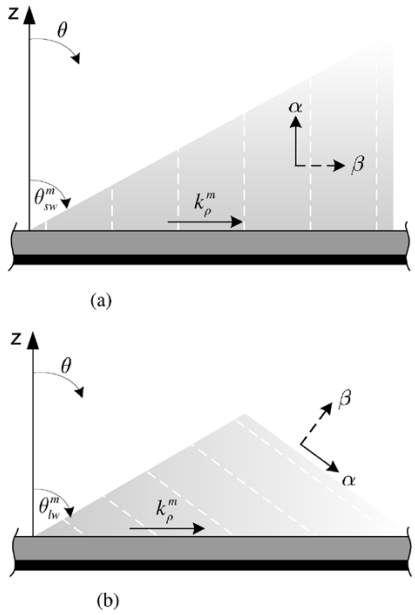

Fig. 6. Vertical plane cuts showing the right propagating surface and leaky waves above a grounded substrate; β denotes a propagation constant along the phasefronts and α denotes an attenuation constant, (a) Surface wave ($\theta > \theta_{\mathrm{sw}}^m$), (b) Leaky wave ($\theta > \theta_{\mathrm{lw}}^m$).

E. Floquet Corner-Excited Surface and Leaky Waves

The contribution from the residue of the SW/LW pole of $\bar{G}(k_x, k_y)$ and the saddle point of the exponential term yields the Floquet corner-excited SW/LWs launched via Floquet corner diffraction from the array corners. The Floquet corner-excited SW/LW launched from the corner c_i, formed by the junction of the $\hat{x}$-directed edge e_j and the $\hat{y}$-directed edge $e_{j'}$, respectively, is given by

$$\bar{E}_{kl}^{slw,c_i} = e^{-j\psi_{c_i}} \sum_m \bar{R}_{c_i}^m \cdot \bar{\bar{L}}_{c_i}^m \frac{e^{-jk_\rho^m \rho_{c_i}}}{\sqrt{\rho_{c_i}}} e^{-j\zeta_0^m z} U_{c_i}^m \quad (55)$$

where

$$\bar{R}_{c_i}^m = \mathrm{Res}\{\bar{G}\}|_{(k_\rho = k_\rho^m)} \quad (56)$$

$$\bar{\bar{L}}_{c_i}^m = \sqrt{\frac{k_\rho^m}{2\pi j}} \zeta_0^m \left\{ \bar{\bar{L}}_{c_i}^{m,1} + \bar{\bar{L}}_{c_i}^{m,2} \right\} \quad (57)$$

$$\bar{\bar{L}}_{c_i}^{m,1} = \bar{\bar{I}} B_x^i(k_\rho^m \cos\phi_{e_j}) B_y^i(k_\rho^m \cos\phi_{e_{j'}}) \quad (58)$$

$$\bar{\bar{L}}_{c_i}^{m,2} = -\frac{\varepsilon_{e_j}}{jd_x} \sum_p \bar{\bar{K}}_{e_j}^{mp} \frac{B_y^i(k_y^{mp})}{k_y^{mp}} \frac{[1 - F(k_\rho^m \rho_{c_i} (\sigma_{e_j}^{mp})^2)]}{\sqrt{2}\sigma_{e_j}^{mp}} - \frac{\varepsilon_{e_{j'}}}{jd_y} \sum_q \bar{\bar{K}}_{e_{j'}}^{mq} \frac{B_x^i(k_x^{mq})}{k_x^{mq}} \frac{\left[1 - F\left(k_\rho^m \rho_{c_i} \left(\sigma_{e_{j'}}^{mq}\right)^2\right)\right]}{\sqrt{2}\sigma_{e_{j'}}^{mq}} \quad (59)$$

$$\bar{\bar{K}}_{e_j}^{mp} = \frac{\bar{R}_{c_i}^m \bar{R}_{e_j}^{mp}}{\left|\bar{R}_{c_i}^m\right|^2}; \qquad \bar{\bar{K}}_{e_{j'}}^{mq} = \frac{\bar{R}_{c_i}^m \bar{R}_{e_{j'}}^{mq}}{\left|\bar{R}_{c_i}^m\right|^2}. \quad (60)$$

The $U_{c_i}^m$ in (55) denotes the unit step function defining the shadow boundary of the corner-excited SW/LW modes. The arguments of the $F(.)$ function in (59) are given by

$$\sigma_{e_j}^{mp} = \sqrt{2}\sin\left(\frac{\xi^{mp} - \phi_{e_j}}{2}\right)$$
$$\sigma_{e_{j'}}^{mq} = \sqrt{2}\sin\left(\frac{\xi^{mq} - \phi_{e_{j'}}}{2}\right). \quad (61)$$

The other parameters are defined as $\xi^{mp} = \cos^{-1}(k_x^p/k_\rho^m), \xi^{mq} = \cos^{-1}(k_y^q/k_\rho^m), \phi_{e_j} = \cos^{-1}((x - x'_{c_i})/\rho_{c_i})$, and $\phi_{e_{j'}} = \cos^{-1}((y - y'_{c_i})/\rho_{c_i})$, respectively, where $\rho_{c_i} = [(x - x'_{c_i})^2 + (y - y'_{c_i})^2]^{1/2}$, and $\{x'_{c_i}, y'_{c_i}\}$ are defined as in Section III-C.

The SW/LWs are launched from the array corner due to the Floquet modal corner diffraction discussed previously. These SW/LWs are also similar to those that can exist on the grounded substrate in the absence of the array. The corner-excited SW/LWs have a cylindrical spreading factor along the surface as shown in Fig. 7. They uniformly compensate the discontinuities of the corresponding edge-excited SW/LWs at the shadow boundaries arising at the array corners.

IV. Numerical Results and Discussion

Some numerical examples are shown in this section to demonstrate the accuracy and efficiency of the present DFT-UTD approach for the analysis of the radiation from a finite rectangular planar array of short and thin printed dipoles on an infinite grounded substrate, as illustrated in Fig. 8. The substrate consists of a dielectric material with a dielectric

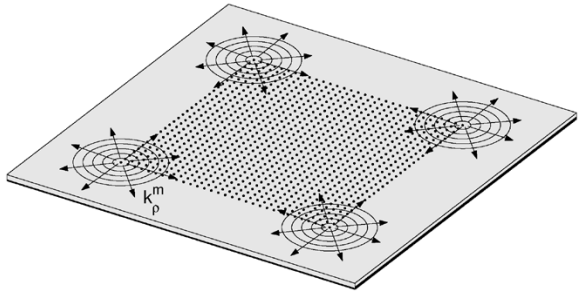

Fig. 7. Ray picture illustrating the corner-excited surface/leaky wave.

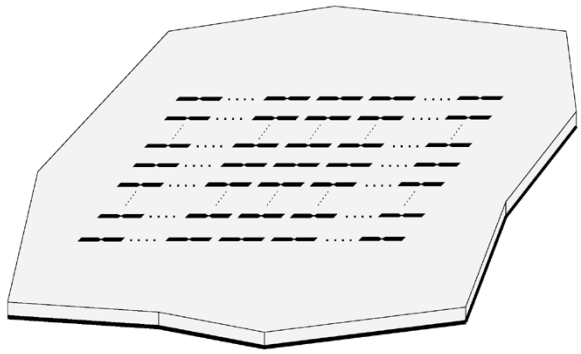

Fig. 8. Geometry of a finite rectangular array of short printed dipoles on an infinite grounded substrate.

constant $\epsilon_r = 2.55$ and has a thickness $d = 0.19\ \lambda_0$, where λ_0 denotes the free space wavelength. The array is composed of 41×41 short printed dipole elements which are oriented in the $\hat{x}$ direction. The dipole length and width are $L = 0.39\ \lambda_0$ and $W = 0.01\ \lambda_0$, respectively. The periodic interelement spacings in the $\hat{x}$ and $\hat{y}$ directions are $d_x = d_y = 0.5\ \lambda_0$. The array is fed with the Gaussian tapered excitation voltage to scan a main beam in the direction $(\theta_0, \phi_0) = (30°, 0°)$. The current on each short and thin printed dipole is approximated locally by a piecewise sinusoidal distribution, and its amplitude is obtained numerically via the rigorous accelerated DFT-MoM solution [12], [13]. The array current distribution obtained from the accelerated DFT-MoM is shown in Fig. 9, and its corresponding DFT spectrum is shown in Fig. 10. The near and far fields of the array are computed by the DFT-UTD ray solution, and are compared to the reference solution obtained via the standard array element-by-element field summation approach.

Fig. 11 illustrates the $\hat{\theta}$ component of the far-field radiation pattern in the scan plane $(\phi = 0°)$ computed by the DFT-UTD ray solution and the reference solution. The DFT-UTD ray solution employs only 81 (4.8 %) dominant DFT terms in the two principal bands of the DFT spectrum out of the total 1,681 terms (equal to the number of array elements). The DFT-UTD ray solution shows a very good agreement with the reference solution. Fig. 12 shows the $\hat{x}$ component of the electric field in the near zone above the array aperture at $(-15\ \lambda_0 \le x \le 15\ \lambda_0, y = 0, z = 5\ \lambda_0)$ in the xz plane. The result obtained from the DFT-UTD ray solution utilizes only 81 dominant DFT terms, and it also compares well with the reference solution.

It is noted that for an $N \times M$ element array, where $N \times M = K$, the conventional array element-by-element field summation approach requires $\mathcal{O}(K)$ operation for the near field calculation. In contrast, the collective DFT-UTD ray solution requires

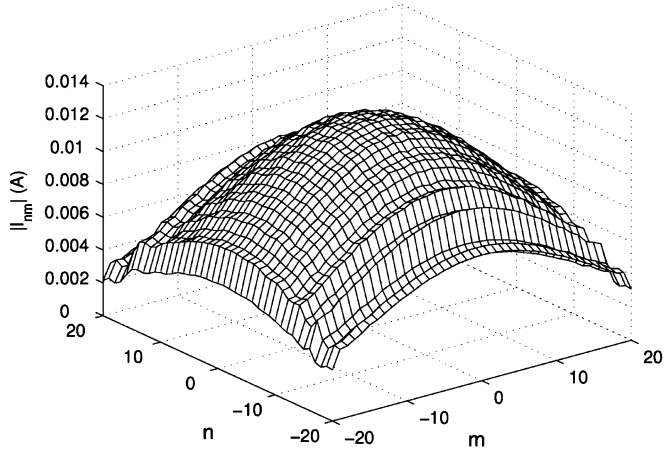

Fig. 9. Array current distribution obtained from the accelerated DFT-MoM solution of the printed dipole array in Fig. 8.

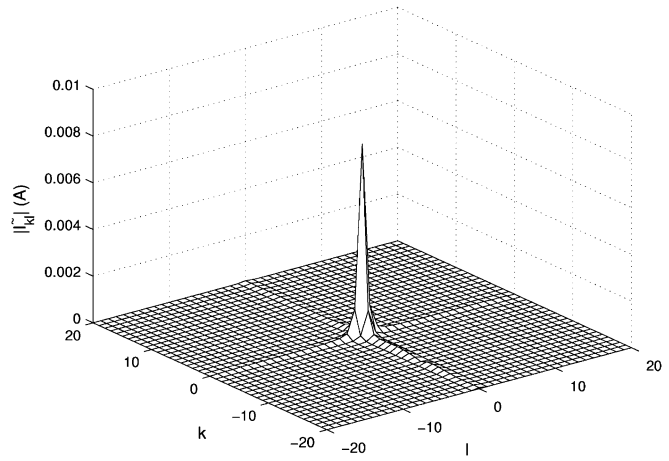

Fig. 10. DFT spectrum of the array current distribution in Fig. 9.

$\mathcal{O}(N_d \times N_r)$ computation, where N_d is the number of dominant DFT terms which is usually a small fraction of K (typically less than 10%), and N_r is the number of the collective UTD rays associated with each DFT term. For the observation region in which only the propagating FWs and their corresponding edge and corner diffracted space waves are important, one requires only 9 rays (1 FW, 4 edge diffracted rays, and 4 corner diffracted rays) associated with each propagating Floquet mode. Typical phased antenna arrays are usually designed to not radiate any grating lobes so that there is only one propagating mode due to each DFT term (It is noted that some discarded nondominant DFT terms may produce only evanescent Floquet modes). For the observation region where the SW/LWs also become important, e.g., near grazing, one need to include a few additional rays of the edge-excited and corner-excited SW/LWs due to each DFT term. It is noted that $N_r \ll K$ for large arrays and N_r is independent of the number of array elements (or the array size). For the far field calculation, the conventional array element-by-element field summation approach requires $\mathcal{O}(K)$ operation. Alternatively, one may employ the FFT to compute the far field at $N_p (N_p \geq K)$ observation points simultaneously, which requires the operational cost of $\mathcal{O}(N_p \log N_p)$, or on average $\mathcal{O}(\log N_p)$ per one observation point. On the other hand, the DFT-UTD ray solution for the far field requires the $\mathcal{O}(N_d)$ operation for each observation point since the far field due to each DFT term can be expressed in closed form.

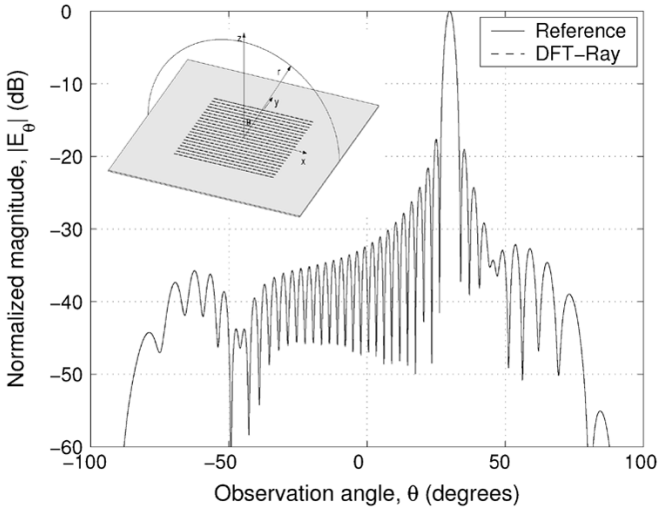

Fig. 11. Normalized magnitude of the $\hat{\theta}$ component of the electric far-field pattern in the E-plane ($\phi = 0^\circ$) obtained via the DFT-UTD ray solution (dash line) and the reference solution (solid line).

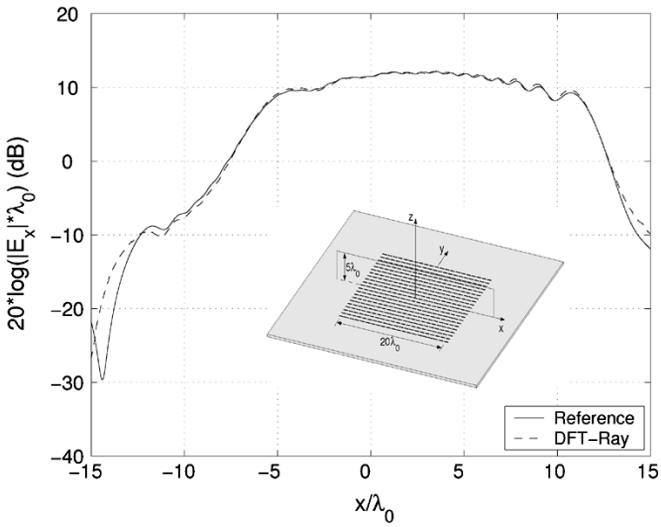

Fig. 12. Magnitude of the $\hat{x}$ component of the electric field in the near zone above the array aperture at ($-15\ \lambda_0 \leq x \leq 15\ \lambda_0, y = 0, z = 5\ \lambda_0$) obtained via the DFT-UTD ray solution (dash line) and the reference solution (solid line).

V. Conclusion

The DFT-based asymptotic closed form UTD representation of the collective fields produced by a finite rectangular planar array of printed antenna elements on an infinite grounded substrate is obtained in this work. A relatively arbitrary realistic array current distribution is expressed in terms of a sequence of simple distributions via the DFT expansion. Each DFT term, which represents a uniform amplitude and linear phased array distribution, produces the collective array field that can be expressed analytically in closed form via the asymptotic ray analysis which provides a simple UTD ray picture for collective array radiation and scattering. A very significant advantage of the DFT expansion for the arbitrary realistic array current distribution (that can be obtained from any rigorous MoM formulation for actual printed array elements) is that, for most prac-

tical phased array excitations, only a relatively few DFT terms remain significant. Hence, the complete DFT expansion can be truncated to include only the dominant terms. Since the UTD ray solution developed here provides the array near and far fields collectively in terms of only a few rays for each of the relatively small number of truncated DFT terms, such an approach is more efficient for field calculations as compared to the conventional array element-by-element field summation approach. The asymptotic UTD ray solution developed here includes a simple physical picture for the collective SW/LW excitation mechanisms that can also exist in printed antenna arrays. Numerical results for the near and far fields of the short printed dipole array based on the DFT-UTD ray solution are seen to compare well with the reference solution.

REFERENCES

[1] B. A. Munk, *Frequency Selective Surfaces: Theory and Design*. New York: Wiley, 2000.

[2] K. A. Shubert and B. A. Munk, "Matching properties of arbitrary large dielectric covered phased array," *IEEE Trans. Antennas Propag.*, vol. AP-31, no. 1, pp. 54–59, Jan. 1983.

[3] A. Ishimaru, R. J. Coe, G. E. Miller, and W. P. Geren, "Finite periodic structure approach to large scanning array problems," *IEEE Trans. Antennas Propag.*, vol. AP-33, no. 11, pp. 1213–1220, Nov. 1985.

[4] A. K. Skrivervik and J. R. Mosig, "Analysis of finite phase arrays of microstrip patches," *IEEE Trans. Antennas Propag.*, vol. 41, no. 8, pp. 1105–1114, Aug. 1993.

[5] L. B. Felsen and L. Carin, "Diffraction theory of frequency- and time-domain scattering by weakly aperiodic truncated thin-wire gratings," *J. Opt. Soc. Amer.*, vol. 11, pp. 1291–1306, 1994.

[6] L. B. Felsen and E. G. Ribas, "Ray theory for scattering by two-dimensional quasiperiodic plane finite arrays," *IEEE Trans. Antennas Propag.*, vol. 44, no. 3, pp. 375–382, Mar. 1996.

[7] F. Capolino, M. Albani, S. Maci, and L. B. Felsen, "Frequency domain Green's function for a planar periodic semi-infinite phased array," *IEEE Trans. Antennas Propag.*, vol. 47, no. 1, Jan. 2000.

[8] F. Capolino, S. Maci, and L. B. Felsen, "Asymptotic high-frequency Green's function for a planar phased sectoral array of dipoles," *Radio Sci.*, vol. 35, pp. 579–593, Mar.–Apr. 2000.

[9] O. A. Civi, P. H. Pathak, H.-T. Chou, and P. Nepa, "A hybrid UTD-MoM for efficient analysis of electromagnetic radiation/scattering from large finite planar arrays," *Radio Sci.*, vol. 35, pp. 607–620, Mar.–Apr. 2000.

[10] L. Carin, L. B. Felsen, and T.-T. Hsu, "High-frequency fields excited by truncated arrays of nonuniformly distributed filamentary scatterers on an infinite dielectric slab: Parameterizing (leaky mode)-(Floquet mode) interaction," *IEEE Trans. Antennas Propagat.*, vol. 44, no. 1, pp. 1–11, Jan. 1996.

[11] A. Polemi, A. Toccafondi, and S. Maci, "High-frequency Green's function for a semi-infinite array of electric dipoles on a grounded slab—Part I: Formulation," *IEEE Trans. Antennas Propag.*, vol. 49, no. 12, pp. 1667–1677, Dec. 2001.

[12] P. Janpugdee, P. H. Pathak, P. Mahachoklertwattana, and R. J. Burkholder, "An accelerated DFP-MoM for the analysis of large fintie periodic antenna arrays in grounded layered media," in *Proc. IEEE AP-S/URSI Int. Symp.*, vol. 3, Monterey, CA, Jun. 2004, pp. 2679–2682.

[13] ——, "An accelerated DFT-MoM for the analysis of large finite periodic antenna arrays ," *IEEE Trans. Antennas Propag.*, vol. 54, no. 1, pp. 279–283, Jan. 2006.

[14] P. Janpugdee, P. H. Pathak, P. Nepa, O. A. Civi, and H.-T. Chou, "Ray analysis of the radiation from a large finite phased array of antennas on a grounded material slab," presented at the USNC/URSI Nat. Radio Science Meeting, Boston, MA, Jul. 8–13, 2001.

[15] A. Polemi, D. Nencini, S. Maci, and A. Toccafondi, "High-frequency Green's function for a sectoral array of electric dipoles on a grounded slab," in *Proc. ICECom Int. Conf.*, Dubrovnik, Croatia, Oct. 2003, pp. 294–299.

[16] E. Martini, A. Toccafondi, S. Maci, and R. Tiberio, "Floquet wave-based diffraction approach for irregularly contoured planar phased arrays," *IEEE Antennas Wireless Propagat. Lett.*, vol. 2, pp. 246–249, 2003.

[17] E. O. Brigham, *The Fast Fourier Transform*. Englewood Cliffs, NJ: Prentice-Hall, 1974.

[18] O. A. Civi, P. H. Pathak, and H.-T. Chou, "On the Poisson sum formula for the analysis of wave radiation and scattering from large finite arrays," *IEEE Trans. Antennas Propag.*, vol. 47, no. 5, pp. 958–959, May 1999.

[19] L. B. Felsen and N. Marcuvitz, *Radiation and Scattering of Waves*. Piscataway, NJ: IEEE Press, 1994.

[20] P. Janpugdee, "An efficient discrete Fourier transform based ray analysis of large finite planar phased arrays," Master's thesis, The Ohio State Univ., 2002.

[21] S. Maci, A. Toccafondi, A. Polemi, and L. B. Felsen, "High-frequency Green's function for a semi-infinite array of electric dipoles on a grounded slab—Part II: Spatial domain parameterization," *IEEE Trans. Antennas Propaga.*, vol. 53, no. 4, pp. 1364–1376, Apr. 2005.

[22] L. B. Felsen, S. Maci, A. Polemi, and A. Toccafondi, "High-frequency Green's function for a semi-infinite array of electric dipoles on an infinite grounded stratified dielectric slab—Part III: Phase-matched wave interactions and numerical results," *IEEE Trans. Antennas Propag.*, vol. 53, no. 5, pp. 1663–1671, May 2005.

[23] R. G. Kouyoumjian and P. H. Pathak, "A uniform geometrical theory of diffraction for an edge in a perfectly conducting surface," *Proc. IEEE*, vol. 62, pp. 1448–1461, Nov. 1974.

[24] J. B. Keller, "Geometrical theory of diffraction," *J. Opt. Soc. Amer.*, vol. 52, pp. 116–130, 1962.

[25] K.-C. Hill, "A UTD solution to the EM scattering by the vertex of a perfectly conducting plane angular sector," Ph.D. dissertation, The Ohio State Univ., 1990.

[26] A. Hessel, *Antenna Theory*, New York: McGraw-Hill, 1969, pt. 2, ch. 19.

Panuwat Janpugdee (S'03) was born on October 12, 1972, in Suratthani, Thailand. He received the B.E. degree in electrical engineering from Chulalongkorn University, Bangkok, Thailand, in 1994, and the M.S. degree in electrical engineering from The Ohio State University, Columbus, OH, in 2002. He is currently working toward the Ph.D. degree in electrical engineering at The Ohio State University.

Since 1998, he has been working as a Graduate Research Associate at the ElectroScience Laboratory, The Ohio State University. His research interests focus on high-frequency and hybrid methods in computational electromagnetics. Currently, he is working on the analysis of large phased antenna arrays integrated into a large complex platform.

Mr. Janpugdee is a member of Phi Kappa Phi.

Prabhakar H. Pathak (M'76–SM'81–F'86) received the M.S. and Ph.D. degrees in electrical engineering from The Ohio State University, Columbus, in 1970 and 1973, respectively.

Currently, he is a Professor at The Ohio State University. His main area of research is in the development of uniform asymptotic theories (frequency and time domain) and hybrid methods for the analysis of large electromagnetic antenna and scattering problems of engineering interest. He is one of the major contributors to the development of the uniform geometrical theory of diffraction (UTD). He has also analyzed the scattering from large inlet cavities via hybrid ray and modal/numerical methods. Recently he has developed new fast asymptotic/hybrid methods which provide physical insights into the radiation mechanisms, for the analysis/design of modern satellite antennas such as large reflector systems and large phased arrays. Some of this work involves the use of Gaussian beams and their diffraction for large reflector systems, as well as developing a UTD and hybrid analysis for large finite arrays which can exhibit surface wave effects. He has presented many short courses and invited lectures both in the U.S. and abroad. He has published over 100 journal and conference papers, as well as authored/co-authored chapters for seven books.

Prof. Pathak is an elected member of U.S. Commission B of the International Union of Radio Science (URSI). He received the 1996 Schelkunoff Best Paper Award from the IEEE TRANSACTIONS ON ANTENNAS AND PROPAGATION, the George Sinclair Award for his research contributions to the ElectroScience Laboratory, The Ohio State University, in 1996 and the Lumley Research Award in 1990, 1994, and 1998, from the College of Engineering, The Ohio State University. In July 2000, he was awarded the IEEE Third Millennium Medal from the Antennas and Propagation Society. He has chaired and organized many technical sessions at national and international conferences. He was invited to serve as an IEEE Distinguished Lecturer from 1991 through 1993. He also served as the Chair of the IEEE Antennas and Propagation Distinguished Lecturer Program during 1999–2005. Prior to 1993, he served as an Associate Editor of the IEEE TRANSACTIONS ON ANTENNAS AND PROPAGATION for two consecutive terms.